Building and Environment 64 (2013) 26–37

Contents lists available at SciVerse ScienceDirect

Building and Environment

journal homepage: www.elsevier.com/locate/buildenv

A state-space model for dynamic response of indoor air temperature and humidity

Ye Yao [a,*], Kun Yang [a], Mengwei Huang [a], Liangzhu Wang [b]

[a] Institute of Refrigeration and Cryogenics, Shanghai Jiao Tong University, No. 800 Dongchuan Rd., Shanghai 200240, China
[b] Department of Building, Civil and Environmental Engineering, Concordia University, Montreal, QC H3G1M8, Canada

ARTICLE INFO

Article history:
Received 7 December 2012
Received in revised form
10 March 2013
Accepted 14 March 2013

Keywords:
State-space model
Dynamic response
Indoor air zone
Temperature
Humidity

ABSTRACT

The real-time control of indoor thermal conditions needs dynamic models of air temperature and humidity in rooms. The single-zone dynamic model may be inappropriate to depict the spatial variations of the air parameters, and the computational fluid dynamics model (CFD) is too computationally costly for real-time applications. In comparison, the multi-zone model, which models a space by several zones, may be a better choice. This paper presents a three-zone dynamic model to investigate the dynamic behaviors of indoor air temperature and humidity. By the means of linear approximation, the ordinary differential equations describing the dynamic thermal behaviors of indoor air are transformed into a state space form. The state equation is solved analytically, and the calculated results are then compared to a series of dynamic response experiments. It shows that the dynamic model developed in this paper predicts well the dynamic thermal responses of air in different indoor zones. The average errors of the calculated results compared with the experimental data are all less than 12% for the transient response with a time period of 2400 s. This paper also demonstrated the developed room model to simulate the transient responses of the indoor air temperatures and humidity ratios under different perturbations including a step change of supply air temperature, supply air flow rate, indoor occupant number and ambient temperature. The proposed modeling procedure may be especially useful for the development of the dynamic toolbox for the control design of HVAC components.

1. Introduction

The air-conditioned room is an important component in a whole HVAC system. The air-conditioning system is usually designed with respect to the thermal characteristic of the air-conditioned room, and the system control scheme is developed based on the requirement of the indoor thermal environment. Real-time control of the air conditioning system needs dynamic models of temperature distribution in rooms. As early as 1980s, Metha et al. [1] established a dynamic response model for the indoor air temperatures assuming that the air in the room is well mixed and the heat capacity of furniture is included in the air. Borresen et al. [2] discussed several simplified dynamic room models in which the thermal interaction between room air and surrounding walls are taken into account in different ways, e.g. the influence of the walls on the indoor air temperatures is neglected; the convective heat transfer between the air and the walls is considered; and the walls' thermal response time is used for the dynamic simulation. The study concluded that the choice of the simplified level employed depends on how closely the long-term responses and steady-state values fit the actual room response. Roberts et al. [3] developed a dynamic model for a single-zone environmental chamber in the heating mode. Experiments were performed in the chamber to measure the air temperature response while controlling the flow rate. Results showed that the response of the nonlinear feedback system was sensitive to changes in parameters such as heat input. Ahmed et al. [4] set up a room model particularly for the development of a laboratory simulator. The room model includes algorithms to generate both steady and transient pressure and thermal responses under various operating conditions. The room pressure was associated with the lab safety constraints while the thermal response was related to occupant comfort. Yang et al. [5] developed an optimized artificial neural network model (ANN) to predict room air temperature and the descending time of room air temperature to determine the optimal stop time of HVAC equipment. The ANN model was developed based on the algorithm of back-propagation learning, which has the optimized values of learning rate, moment, bias, number of hidden layer, and number of neurons

* Corresponding author. Tel.: +86 21 13641943577.
E-mail addresses: yeyao10000@163.com, yeyao10000@sjtu.edu.cn (Y. Yao).

0360-1323/$ – see front matter © 2013 Elsevier Ltd. All rights reserved.
http://dx.doi.org/10.1016/j.buildenv.2013.03.009

Nomenclature

A	Area, m^2
a	Convective heat transfer coefficient, $W/(m^2\ ^\circ C)$
c	Mass specific heat, $J/(kg\ ^oC)$
E_{body}	Metabolic rate of human body, W/m^2
G	Mass flow rate of air or water, kg/s
H_{body}	Height of human body, m
h	Enthalpy, J/kg
I_{sol}	Solar radiant intensity, W/m^2
M_{body}	Mass of human body, kg
ΔM	Moisture gain rate, kg/s
ΔQ	Energy gain rate, W
t^oC	Temperature,
V	Volume, m^3
W	Humidity ratio, g/(kg dry air)
α_ρ	Absorption factor of solar radiation
τ	Time, s
ρ	Density, kg/m^3
λ	Coefficient of heat conductivity, $W/(m\ ^\circ C)$
δ	Thickness, m

Subscripts

a	Air
$an-ar$	Air layer between the work zone and the air-return zone
$as-an$	Air layer between the air-supply zone and the work zone
i	Inlet of air-supply zone
n	Work zone
r	Air-return zone
riw	Internal wall
rew	External wall
rq	Indoor heat source
s	Air-supply zone

of hidden layer. Mustafaraj et al. [6] investigated Box–Jenkins (BJ), autoregressive with external inputs (ARX), autoregressive moving average with external inputs (ARMAX) and output error (OE) models to identify the thermal behavior of an office room in a modern commercial building in London. Their study manifests that these numerical models can all be potentially used for improving the performance of the thermal environment control system. The ARMAX method was also employed by Wu et al. [7] to predict the room temperature variations for both short-term and long-term periods. All the room models mentioned above belong to the single-zone model, i.e. one air node representing the whole air status in the room. The single-zone model has been widely used in many HVAC simulation tools, like TRNSYS, HVACSIM and BLAST [8], due to its simple practicality.

To investigate the detailed indoor air flow and temperature distribution, the computational fluid dynamics (CFD) method is often employed and demonstrated in much literature [9–14]. Some researchers also managed to use the CFD method to develop the dynamic model of indoor air. Chen and Peng [15] firstly studied the indoor dynamic temperature distributions by using a fixed-flow-field CFD model in which the room thermal response and indoor air distribution were computed considering the outdoor air temperature, solar radiation, indoor heat sources and other thermal boundary conditions. Although the CFD results were shown to agree well with the experimental data, the calculation was too time consuming and therefore not cost effective for the study of the dynamic thermal characteristic of the room and the control system. To make CFD models more suitable for the on-line control, Zerihun et al. [16] extended a complex CFD simulation model with a simplified, low-order representation of the process using a mathematical identification technique. The reduced-order model may be of important practical advantage for control applications especially when experimentation is difficult or in some extreme cases impossible, Sun et al. [17] studied a CFD-based test method combining a ventilated room with a dynamic ventilation and control system. The approach of merging the traditional ventilation and control system with CFD simulation to test indoor ventilation performance will undoubtedly provide new possibilities for testing and evaluating the ventilation control processes. But, there still face great challenge for the CFD method in the control applications because too many factors (i.e., the turbulence model, the numerical truncations, difficulties in setting boundary conditions and limitations of computer capacity) will lead to the poor CFD results and cause a control failure.

A multi-zone model simplifies the CFD model by dividing a room, which is otherwise modeled in CFD by thousands of finite volumes, into several air zones each of which is assumed to be well-mixed as one air node. Usually, the room air zones are divided in terms of the air momentum and the air flow rate based on the degradation of fluid mechanics equations [18]. Compared to the single-zone model, the simplified multi-zone room model is much closer to the actual situation while saving a great amount of computational time of the CFD model. So, it should be a good choice for the study of the dynamic thermal characteristic of indoor air and the control system design [19–21].

Most of the previous dynamic room models in the literature focused on the indoor air temperatures and ignored the indoor air humidity. In this study, we develop a dynamic room model for both indoor air temperature and humidity. By the means of linear approximation, the ordinary differential equations describing the room air thermal dynamics are converted into the state-space form. The analytical solution to the state equation is obtained, and the state-space room model is validated by experiments. Then, the room model is used to simulate the dynamic response of indoor air thermal conditions under different perturbations based on which the thermal response characteristics of air in the room are analyzed.

The potential benefits of state-space method used for the modeling in this study mainly lie in the following aspects:

- Unlike the ANN, ARMAX and ARX model, the state-space method is a mechanism one which can allow us to understand the essences of dynamic relationship between the input perturbations and the output response variables of the system.
- The state-space model is flexible and easy to simulate the transient response of multi-input-and-multi-output system (MIMO) to which the room belongs.
- The state-space model can not only provide information of the system outputs, but also that of the state variables that can be used as feedback mechanism to improve the control performance.
- Lastly, the state-space model is an important base for the development of MPC (model based controller) that may have good applications in the HVAC fields [22–24].

2. Model development

2.1. Assumptions

For the convenience of modeling, the following assumptions are necessarily made:

- As shown in Fig. 1, the room is separated into three typical zones, i.e. the air-supply, the work and the air-return zones. Each air zone is fully mixed and is described by one state.
- The surface temperature of each inner and external wall is all described with a lumped value. The heat transfer from the external walls only affects the air in the work zone, and there is no heat and mass transfer between the air-supply and the air-return zones.
- In the air-supply zone, light bulbs are the only heat sources defined by a constant surface temperature during the transient response simulation. No moisture sources exist in the air-supply zone.
- In the work zone, the heat sources are electrical appliances and people indoors, and the moisture sources are evaporative water from the skin and from the respiration of human indoors. The surface temperature of all the heat sources is assumed to be constant during the dynamic response simulation.
- There are no heat and moisture sources in the air-return zone.
- The radiant heat transfer between walls and objects in the room is negligible. The convective heat transfer coefficients between the walls or the heat sources and the adjacent air are considered to be constant during the dynamic response simulation.

2.2. Basic equations

Based on the above assumptions, the energy and mass equations for the room air and walls in different zones can be established according to the law of energy and mass conservation.

For the air-supply zone

$$\rho_a V_{a,s}\frac{\mathrm{d}h_{a,s}}{\mathrm{d}\tau} = G_{a,i}(h_{a,i} - h_{a,s}) + \Delta Q_{a,s} \tag{1}$$

$$\rho_a V_{a,s}\frac{\mathrm{d}W_{a,s}}{\mathrm{d}\tau} = G_{a,i}(W_{a,i} - W_{a,s}) \tag{2}$$

$$c_{riw,s}\rho_{riw}V_{riw,s}\frac{\mathrm{d}t_{riw,s}}{\mathrm{d}\tau} = a_{riw,s}A_{riw,s}(t_{a,s} - t_{riw,s}) \tag{3}$$

For the work zone

$$\rho_a V_{a,n}\frac{\mathrm{d}h_{a,n}}{\mathrm{d}\tau} = G_{a,i}(h_{a,s} - h_{a,n}) + \Delta Q_{a,n} \tag{4}$$

$$\rho_a V_{a,n}\frac{\mathrm{d}W_{a,n}}{\mathrm{d}\tau} = G_{a,i}(W_{a,s} - W_{a,n}) + \Delta M_{Wa,n} \tag{5}$$

$$c_{riw,n}\rho_{riw}V_{riw,n}\frac{\mathrm{d}t_{riw,n}}{\mathrm{d}\tau} = a_{riw,n}A_{riw,n}(t_{a,n} - t_{riw,n}) \tag{6}$$

$$c_{rew,n}\rho_{rew}V_{rew,n}\frac{\mathrm{d}t_{rew,n}}{\mathrm{d}\tau} = a_{rew,n}A_{rew,n}(t_{a,n} - t_{rew,n}) + \frac{\lambda_{rew}A_{rew,n}}{\delta_{rew}}(t_{rew,o} - t_{rew,n}) \tag{7}$$

For the air-return zone

$$\rho_a V_{a,r}\frac{\mathrm{d}h_{a,r}}{\mathrm{d}\tau} = G_{a,i}(h_{a,n} - h_{a,r}) + \Delta Q_{a,r} \tag{8}$$

$$\rho_a V_{a,r}\frac{\mathrm{d}W_{a,r}}{\mathrm{d}\tau} = G_{a,i}(W_{a,n} - W_{a,r}) \tag{9}$$

$$c_{riw,r}\rho_{riw}V_{riw,r}\frac{\mathrm{d}t_{riw,r}}{\mathrm{d}\tau} = a_{riw,r}A_{riw,r}(t_{a,r} - t_{riw,r}) \tag{10}$$

In Eqs. (1), (4) and (10) $\Delta Q_{a,s}$,$\Delta Q_{a,n}$ and $\Delta Q_{a,r}$is the heat gain rate of air corresponding to the three room zones (i.e., the air-supply, the work and the air-return zone).

$$\Delta Q_{a,s} = a_{riw,s}A_{riw,s}(t_{riw,s} - t_{a,s}) + a_{as-an}A_{as-an}(t_{a,n} - t_{a,s}) + a_{rq,s}A_{rq,s}(t_{rq,s} - t_{a,s}) \tag{11}$$

$$\Delta Q_{a,n} = a_{riw,n}A_{riw,n}(t_{riw,n} - t_{a,n}) + a_{rew,n}A_{rew,n}(t_{rew,n} - t_{a,n}) + a_{as-an}A_{as-an}(t_{a,s} - t_{a,n}) + a_{an-ar}A_{an-ar}(t_{a,r} - t_{a,n}) + \sum_{i=1}^{k}\left[a_{rq,n}A_{rq,n}^{(i)}\left(t_{rq,n}^{(i)} - t_{a,n}\right)\right] + G_{res}(h_{exhale} - h_{a,n}) \tag{12}$$

$$\Delta Q_{a,r,2} = a_{riw,r}A_{riw,,r}(t_{riw,r} - t_{a,r}) + a_{an-ar}A_{an-ar}(t_{a,n} - t_{a,r}) \tag{13}$$

The superscript '*i*' in Eq. (12) denotes the *i*th indoor heat source. The enthalpy of the exhaled airh_{exhale}, is related to the temperature (t_{exhale}) and humidity ratio (W_{exhale}) of the exhaled air. For typical indoor environments ($t_{a,n}$=25 °C), the exhaled temperature and humidity ratio are given in terms of ambient conditions [25]:

$$t_{exhale} = 32.6 + 0.066t_{a,n} \tag{14}$$

$$W_{exhale} = 0.02933 + 0.2W_{a,n} \tag{15}$$

Please note that the unit of $W_{a,n}$in Eq. (15) is kg/(kg dryair). The pulmonary ventilation rateG_{res}, is primarily a function of metabolic rate as below [25]:

$$G_{res} = C_{res}E_{body}A_{rq,n}^{(1)} \tag{16}$$

where, C_{res} is a proportionality constant (1.43×10^{-6} kg/J);E_{body} is metabolic rate, W/m^2; $A^{(1)}$is body surface area of occupant indoors (m^2), which is calculated by Eq. (17) [25].

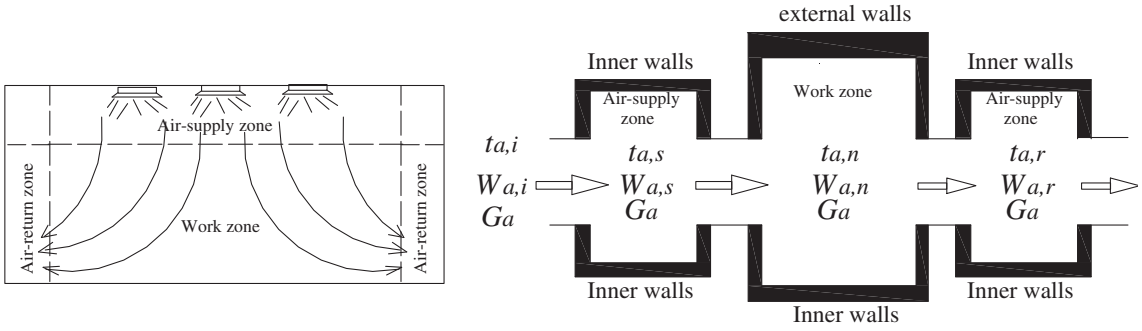

Fig. 1. Schematic for the air-conditioned room

$$A_{rq,n}^{(1)} = 0.202 M_{body}^{0.425} H_{body}^{0.725} \tag{17}$$

where, M_{body} and $H_{body}$is the weight and the height of the occupant.

Moisture gain rate of the air in the work zone$\Delta M_{Wa,n}$, may be calculated by [25]:

$$\begin{aligned}\Delta M_{Wa,n} &= G_{res}\left(W_{exhale} - W_{a,n}\right) \\ &= C_{res} M_{body} A_{rq,n}^{(1)}\left(0.02933 - 0.8 W_{a,n}\right)\end{aligned} \tag{18}$$

The external surface temperature of external walls$t_{rew,o}$, is affected by the ambient air temperature and solar radiation intensity on the walls, which may be calculated by [25]:

$$t_{rew,o} = t_{a,out} + \alpha_{\rho,rew} I_{sol} / a_{rew,o} \tag{19}$$

The air enthalpyh_a, in Eqs. (1), (4) and (8) is a function of temperature (t_a) and humidity (W_a), which is expressed by Eq. (20).

$$h_a = c_a t_a + \left(2.5 \times 10^6 + c_a t_a\right) W_a \tag{20}$$

where, $c_a = 1005$J/(kg °C); $c_{a.w} = 1840$ J/(kg °C).

Since $c_{a.w} t_a << 2.5 \times 10^6$, the air enthalpy$h_a$, may be simplified as Eq. (21) for the decoupling of the temperature (t_a) from the humidity (W_a) in Eqs. (1), (4) and (8).

$$h_a = c_a t_a + \beta_2 W_a \tag{21}$$

where, β_2 is a constant that approximately equals to2.5×10^6.

The division of the room air volume into air zones ($V_{a,s}, V_{a,n}, V_{a,r}$) is determined based on the air flow pattern and the steady state temperature field calculated with the CFD method [18,19]. Meanwhile, the actual situations should be fully considered in the division of the indoor air zones. Normally, the work zone is less than 2.0 m in height [26].

The other critical parameters of the zonal model include the heat transfer coefficients between the air and the internal surface of the room walls ($a_{riw,s}$,$a_{riw,n}$,$a_{riw,r}$), the indoor heat sources ($a_{rq,s}$,$a_{rq,n}$), and the heat transfer coefficients between two adjacent air zones (a_{an-ar},a_{as-an}). Basically, These heat transfer coefficients are originally obtained from the relevant literature [27,28], and need to be adjusted according to the comparisons of the calculated results and the experimental data.

2.3. State-space model formulation

There are two types of parameters in the model: the constants and the variables. The constants are the basic parameters including the size of room envelope and the contact area among the indoor air zones. The variables include the states (temperature and humidity) of air in different zones, the temperatures of walls and indoor heat sources, the mass flow rate of supply air, the ambient air temperature and the solar radiation intensity, and the surface area of indoor heat sources as well as the total respiratory volume of occupants indoors. It is noted here that the change of surface area of indoor heat sources is used to simulate the disturbances from indoor heat gains.

In order to convert Eqs. (1)–(10) into a state-space model, the variables are written as the summation of initial value (θ_o) and an increment ($\Delta\theta$), i.e.$\theta = \theta_o + \Delta\theta$. Meanwhile, the high-order item '$\Delta\theta_1\Delta\theta_2$' in all the equations are omitted to accomplish the linearization. Thus, Eqs. (1)–(10) can be linearized, respectively, as below:

$$\begin{aligned}T_{tas}\frac{\mathrm{d}\Delta t_{a,s}}{\mathrm{d}\tau} &= X_{tas,1}\Delta t_{a,s} + X_{tas,2}\Delta t_{a,i} + X_{tas,3}\Delta t_{riw,s} + X_{tas,4}\Delta t_{a,n} \\ &\quad + X_{tas,5}\Delta G_{a,i}\end{aligned} \tag{22}$$

$$T_{was}\frac{\mathrm{d}\Delta W_{a,s}}{\mathrm{d}\tau} = X_{was,1}\Delta W_{a,s} + X_{was,2}\Delta W_{a,i} + X_{was,3}\Delta G_{a,i} \tag{23}$$

$$T_{riws}\frac{\mathrm{d}\Delta t_{riw,s}}{\mathrm{d}\tau} = X_{riws,1}\Delta t_{a,s} + X_{riws,2}\Delta t_{riw,s} \tag{24}$$

$$\begin{aligned}T_{\tan}\frac{\mathrm{d}\Delta t_{a,n}}{\mathrm{d}\tau} &= X_{\tan,1}\Delta t_{a,s} + X_{\tan,2}\Delta t_{a,n} + X_{\tan,3}\Delta t_{riw,n} \\ &\quad + X_{\tan,4}\Delta_{rew,n} + X_{\tan,5}\Delta t_{a,r} + X_{\tan,6}\Delta G_{a,i} \\ &\quad + \sum_{i=1}^{k}\left[X_{\tan,7}^{(i)}\Delta A_{rq,n}^{(i)}\right]\end{aligned} \tag{25}$$

$$\begin{aligned}T_{wan}\frac{\mathrm{d}\Delta W_{a,n}}{\mathrm{d}\tau} &= X_{wan,1}\Delta W_{a,s} + X_{wan,2}\Delta W_{a,n} + X_{wan,3}\Delta G_{a,i} \\ &\quad + X_{wan,4}\Delta A_{rq,n}^{(1)}\end{aligned} \tag{26}$$

$$T_{triwn}\frac{\mathrm{d}\Delta t_{riw,n}}{\mathrm{d}\tau} = X_{triwn,1}\Delta t_{a,n} + X_{triwn,2}\Delta t_{riw,n} \tag{27}$$

$$\begin{aligned}T_{trewn}\frac{\mathrm{d}\Delta t_{rew,n}}{\mathrm{d}\tau} &= X_{trewn,1}\Delta t_{a,n} + X_{trewn,2}\Delta t_{rew,n} + X_{trewn,3}\Delta t_{a,out} \\ &\quad + X_{trewn,4}\Delta I_{sol}\end{aligned} \tag{28}$$

$$T_{tar}\frac{\mathrm{d}\Delta t_{a,r}}{\mathrm{d}\tau} = X_{tar,1}\Delta t_{a,n} + X_{tar,2}\Delta t_{a,r} + X_{tar,3}\Delta t_{riw,r} + X_{tar,4}\Delta G_{a,i} \tag{29}$$

$$T_{war}\frac{d\Delta W_{a,r}}{d\tau} = X_{war,1}\Delta W_{a,n} + X_{war,2}\Delta W_{a,r} + X_{war,3}\Delta G_{a,i} \quad (30)$$

$$T_{triwr}\frac{d\Delta t_{riw,r}}{d\tau} = X_{triwr,1}\Delta t_{a,r} + X_{triwr,2}\Delta t_{riw,r} \quad (31)$$

Further, Eqs. (22)–(31) (all the coefficients are listed in Table 1.) can be converted into a representation of state space:

$$\dot{\mathbf{X}}_{room} = A_{room}\cdot\mathbf{X}_{room} + B_{room}\cdot\mathbf{U}_{room} \quad (32)$$

where, $\mathbf{X}_{room}$ and $\mathbf{U}_{room}$is called, respectively, the state and input vector. $A_{room}$and $B_{room}$is called the system and input matrix, respectively.

$$\mathbf{X}_{room} = \left[\Delta t_{a,s}\Delta W_{a,s}\Delta t_{riw,s}\Delta t_{a,n}\Delta W_{a,n}\Delta t_{riw,n}\Delta t_{rew,n}\Delta t_{a,r}\Delta W_{a,r}\Delta t_{riw,r}\right]^T$$

$$\mathbf{U}_{room} = \left[\Delta t_{a,i}\Delta W_{a,i}\Delta G_{a,i}\Delta A^{(1)}_{rq,n}\Delta A^{(2)}_{rq,n}\Delta A^{(i)}_{rq,n}\Delta t_{a,out}\Delta I_{sol}\right]^T$$

When the variables, $\Delta t_{a,s}, \Delta W_{a,s}, \Delta t_{a,n}, \Delta W_{a,n}, \Delta t_{a,r}and\Delta W_{a,r}$, are chosen as the output ones, the output vector can be written as:

$$\mathbf{Y}_{room} = C_{room}\mathbf{X}_{room} \quad (33)$$

where, $\mathbf{Y}_{room} = [\Delta t_{a,s},\ \Delta W_{a,s},\ \Delta t_{a,n},\ \Delta W_{a,n},\ \Delta t_{a,r},\ \Delta W_{a,r}]^T$;

$$C_{room} = \begin{bmatrix} 1&0&0&0&0&0&0&0&0&0\\ 0&1&0&0&0&0&0&0&0&0\\ 0&0&0&1&0&0&0&0&0&0\\ 0&0&0&0&1&0&0&0&0&0\\ 0&0&0&0&0&0&0&1&0&0\\ 0&0&0&0&0&0&0&0&1&0 \end{bmatrix}$$

The matrix A in the state space model contains different heat transfer coefficients which are affected by the air flow rate and turbulence and the free movement of air molecules. To better show the relationship among the input, the state and the output variables, Eqs. (32) and (33) can be illustrated by a directed graph according to the graph theory [29] as shown in Fig. 2. The directed graph consists of vertex set and directed edge set. The vertex set comprises of the input ($u_1, u_2, \ldots, u_m$), the state ($x_1, x_2, \ldots, x_n$) and the output variables ($y_1, y_2, \ldots, y_r$). The directed edges reflect the

$$A_{room} = \begin{bmatrix} X_{tas,1}/T_{tas} & 0 & X_{tas,3}/T_{tas} & X_{tas,4}/T_{tas} & 0 & 0 & 0 & 0 & 0 & 0\\ 0 & X_{was,1}/T_{was} & 0 & 0 & 0 & 0 & 0 & 0 & 0 & 0\\ X_{triws,1}/T_{triws} & 0 & X_{triws,2}/T_{triws} & 0 & 0 & 0 & 0 & 0 & 0 & 0\\ X_{tan,1}/T_{tan} & 0 & 0 & X_{tan,2}/T_{tan} & 0 & X_{tan,3}/T_{tan} & X_{tan,4}/T_{tan} & X_{tan,5}/T_{tan} & 0 & 0\\ 0 & X_{wan,1}/T_{wan} & 0 & 0 & X_{wan,2}/T_{wan} & 0 & 0 & 0 & 0 & 0\\ 0 & 0 & 0 & X_{triwn,1}/T_{triwn} & 0 & X_{triwn,2}/T_{triwn} & 0 & 0 & 0 & 0\\ 0 & 0 & 0 & X_{trewn,1}/T_{trewn} & 0 & 0 & X_{trewn,2}/T_{trewn} & 0 & 0 & 0\\ 0 & 0 & 0 & X_{tar,1}/T_{tar} & 0 & 0 & 0 & X_{tar,2}/T_{tar} & 0 & X_{tar,3}/T_{tar}\\ 0 & 0 & 0 & 0 & X_{war,1}/T_{war} & 0 & 0 & 0 & X_{war,2}/T_{war} & 0\\ 0 & 0 & 0 & 0 & 0 & 0 & 0 & X_{triwr,1}/T_{triwr} & 0 & X_{triwr,2}/T_{triwr} \end{bmatrix}$$

$$B_{room} = \begin{bmatrix} X_{tas,2}/T_{tas} & 0 & X_{tas,5}/T_{tas} & 0 & 0 & 0 & 0 & 0 & 0\\ 0 & X_{was,2}/T_{was} & X_{was,3}/T_{was} & 0 & 0 & 0 & 0 & 0 & 0\\ 0 & 0 & 0 & 0 & 0 & 0 & 0 & 0 & 0\\ 0 & 0 & X_{tan,6}/T_{tan} & X^{(1)}_{tan,7}/T_{tan} & X^{(2)}_{tan,7}/T_{tan} & \cdots & X^{(i)}_{tan,7}/T_{tan} & 0 & 0\\ 0 & 0 & X_{wan,3}/T_{wan} & X_{wan,4}/T_{wan} & 0 & 0 & 0 & 0 & 0\\ 0 & 0 & 0 & 0 & 0 & 0 & 0 & 0 & 0\\ 0 & 0 & 0 & 0 & 0 & 0 & 0 & X_{trewn,3}/T_{trewn} & X_{trewn,4}/T_{trewn}\\ 0 & 0 & X_{tar,4}/T_{tar} & 0 & 0 & 0 & 0 & 0 & 0\\ 0 & 0 & X_{tar,4}/T_{tar} & 0 & 0 & 0 & 0 & 0 & 0\\ 0 & 0 & 0 & 0 & 0 & 0 & 0 & 0 & 0 \end{bmatrix}$$

Table 1
Coefficients in Eqs. (22)–(31).

Equation	Formula of coefficients
Eq. (22)	$T_{tas} = c_a\rho_a V_{a,s}$; $X_{tas,1} = -[c_a(G_{a,i})_o + a_{riw,s}A_{riw,s} + a_{as-an}A_{as-an} + a_{rq,s}(A_{rq,s})_o]$; $X_{tas,2} = c_a(G_{a,i})_o$; $X_{tas,3} = a_{riw,s}A_{riw,s}$; $X_{tas,4} = a_{as-an}A_{as-an}$; $X_{tas,5} = c_a(t_{a,i} - t_{a,s})_o$.
Eq. (23)	$T_{was} = \rho_a V_{a,s}$; $X_{was,1} = -(G_{a,i})_o$; $X_{was,2} = (G_{a,i})_o$; $X_{was,3} = (W_{a,i} - W_{a,s})_o$.
Eq. (24)	$T_{triws} = c_{riw,s}\rho_{riw}V_{riw,s}$; $X_{triws,1} = a_{riw,s}A_{riw,s}$; $X_{triws,2} = -a_{riw,s}A_{riw,s}$.
Eq. (25)	$T_{\tan} = c_a\rho_a V_{a,n}$; $X_{\tan,1} = c_a(G_{a,i})_o + a_{as-an}A_{as-an}$; $X_{\tan,2} = -[c_a(G_{a,i})_o + 0.934c_a C_{res}M_{body}A_{rq,n}^{(1)} + a_{riw,n}A_{riw,n} + a_{rew,n}A_{rew,n} + a_{as-an}A_{as-an} + a_{an-ar}A_{an-ar} + \sum_{i=1}^{k}[a_{rq,n}(A_{rq,n}^{(i)})_o]]$; $X_{\tan,3} = a_{riw,n}A_{riw,n}$; $X_{\tan,4} = a_{rew,n}A_{rew,n}$; $X_{\tan,5} = a_{an-ar}A_{an-ar}$; $X_{\tan,6} = c_a(t_{a,s} - t_{a,n})_o$; $X_{\tan,7}^{(i)} = a_{rq,n}[t_{rq,n}^{(i)} - t_{a,n}]_o$.
Eq. (26)	$T_{wan} = \rho_a V_{a,n}$; $X_{wan,1} = (G_{a,i})_o$; $X_{wan,2} = [-0.8C_{res}M_{body}A_{rq,n}^{(1)} - G_{a,i}]_o$; $X_{wan,3} = (W_{a,s} - W_{a,n})_o$; $X_{wan,4} = C_{res}M_{body}(0.02933 - 0.8W_{a,n})_o$.
Eq. (27)	$T_{triwn} = c_{riw,n}\rho_{riw}V_{riw,n}$; $X_{triwn,1} = a_{riw,n}A_{riw,n}$; $X_{triwn,2} = -a_{riw,n}A_{riw,n}$.
Eq. (28)	$T_{trewn} = c_{rew,n}\rho_{rew}V_{rew,n}$; $X_{trewn,1} = a_{rew,n}A_{rew,n}$; $X_{trewn,2} = -a_{rew,n}A_{rew,n} - \lambda_{rew}A_{rew,n}/\delta_{rew}$; $X_{trewn,3} = \lambda_{rew}A_{rew,n}/\delta_{rew}$; $X_{trewn,4} = \alpha_{\rho,rew}\lambda_{rew}A_{rew,n}/(a_{rew,o}\delta_{rew})$.
Eq. (29)	$T_{tar} = c_a\rho_a V_{a,r}$; $X_{tar,1} = c_a(G_{a,i})_o + a_{an-ar}A_{an-ar}$; $X_{tar,2} = -[a_{riw,r}A_{riw,r} + c_a(G_{a,i})_o + a_{an-ar}A_{an-ar}]$; $X_{tar,3} = a_{riw,r}A_{riw,r}$; $X_{tar,4} = c_a(t_{a,n} - t_{a,r})_o$.
Eq. (30)	$T_{war} = \rho_a V_{a,r}$; $X_{war,1} = (G_{a,i})_o$; $X_{war,2} = -(G_{a,i})_o$; $X_{war,3} = (W_{a,n} - W_{a,r})_o$.
Eq. (31)	$T_{triwr} = c_{riw,r}\rho_{riw}V_{riw,r}$; $X_{triwr,1} = a_{riw,r}A_{riw,r}$; $X_{triwr,2} = -a_{riw,r}A_{riw,r}$.

relationship among these variables, e.g. the directed edge starting from the ith vertex to the jth one means the ith variable directly affects the jth. The directed graph can help us better understand how the perturbations of the input variables produce influence on the output ones. For example, Fig. 2 shows that the supply air flow rate ($G_{a,i}$) affects directly the conditions of air in all zones, whereas indirectly the internal surface of walls. Similarly, the outside air temperature and the solar radiant intensity on the external walls influence directly the conditions of air in the work zone while affecting the conditions of air in the air-return zone indirectly.

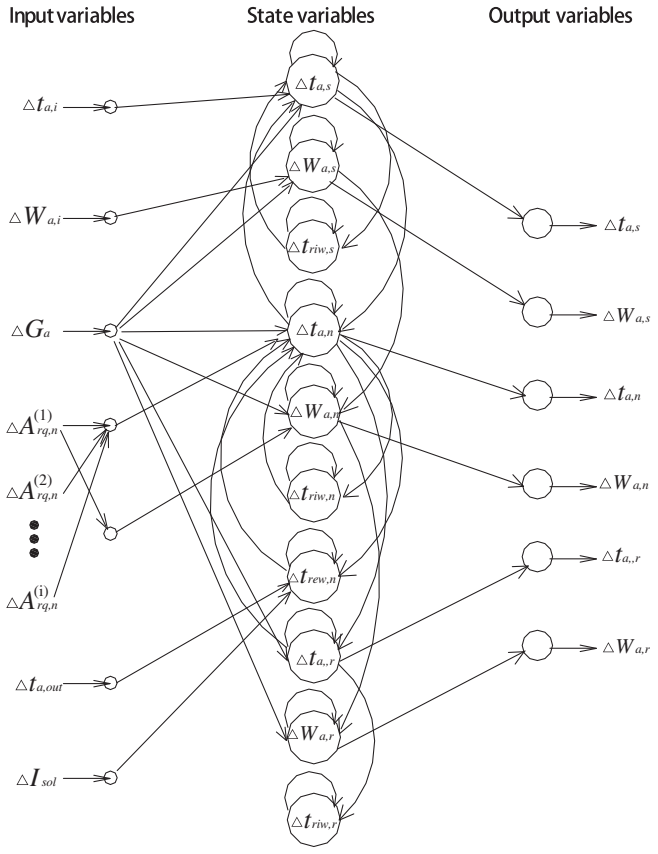

Fig. 2. Directed graph for the state-space model of room

The analytic solution to Eq. (32) at the time step τ_1 can be written as below [30]:

$$\mathbf{X}_{room} = \varphi(\tau)\mathbf{X}_{room}(0) + \int_0^{\tau_1} \varphi(\tau - \tau_1)B_{room}\mathbf{U}_{room}(\tau)d\tau \qquad (34)$$

where, $\varphi(\tau) = Exp(A_{room}\tau)$, which is called the state transition matrix; $\mathbf{X}_{room}(0)$is the initial conditions of the state vector.

3. Model validations

3.1. Experimental system

To validate the above state-space model, an experiment has been conducted in a full-size air-conditioned room. The room is constructed with only internal walls which are made of bricks and limestone with a total thickness of 0.168 m. The air-handling system consists of a water-to-air surface heat exchanger, a ventilator and air supply/return ducts. Two air supply diffuser outlets are located in the upper space of the room for a good air distribution in the room. The supply air temperature can be adjusted by changing the supply water temperature in the heat exchanger.

3.2. Experimental method

The state-space model is validated experimentally in terms of the responses of air temperatures in different indoor zones and air humidity in the air-return zone under perturbations of supply air temperature and humidity. The air flow pattern is pre-calculated with the standard k-ε CFD model to determine the three air zones. As presented in Fig. 3, the dimension for the air-supply, the work and the air-return zone was found to be 0.348 × 0.270 × 0.070 m, 0.348 × 0.270 × 0.180 m and 0.080 × 0.270 × 0.180 m (Length × Width × Height), respectively. The internal surface area of walls corresponding to the three zones is 13.72 m^2, 20.52 m^2 and 3.60 m^2, respectively. The contact area

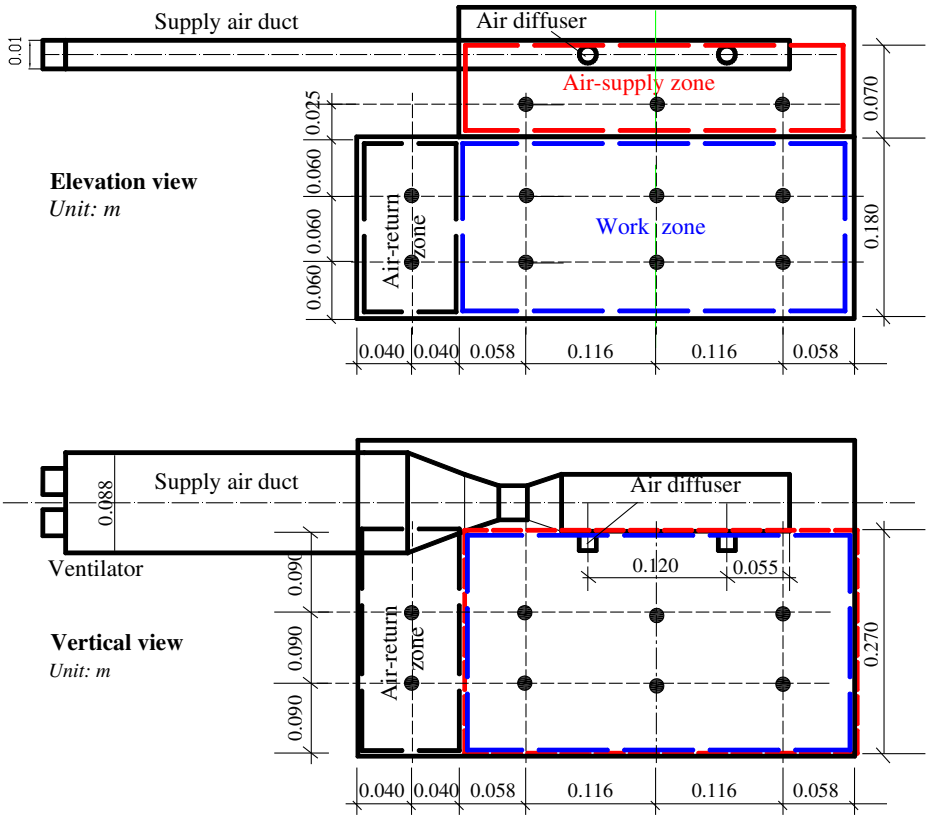

Fig. 3. Test room and detailed positions of temperature sensors

between the work zone and the air-supply zone and the air-return zone is 9.40 m^2 and 4.90 m^2, respectively. Fig. 3 also illustrates the detailed locations of the thermocouples (measurement precision: ±0.1 °C) in the room. The measured air temperature of each zone is taken as the mean values of the test points. A humidity sensor (measurement precision: ±0.8% of the humidity ratio) is placed in the air-return zone to measure the air humidity. The supply air flow rate is measured with a hot-wire anemometer with a measurement precision of ±0.015 m/s. As one of the initial conditions, the internal surface temperatures of the walls were measured by thermocouples (measurement precision: ±0.1 °C) embedded in the internal surface of the walls. The heat sources in the air-supply zone are fluorescent lamps whose surface area is estimated as 0.3 m^2. In the work zone, there are two adults (total body surface area: 3.65 m^2) and a constant-temperature plate heater (surface area: 0.28 m^2). An infrared thermometer (measurement precision: ±0.2 °C) was used to measure the surface temperature of the indoor heat sources. The surface temperature was measured to be 39.6 °C, 35.2 °C and 43.9 °C, respectively, for the lamps, the human bodies and the plate heater during the response experiment.

Two experimental cases have been performed for a time period of 2400 s in both cases. The initial conditions (See Table 2) are measured before the response experiment begins. All the air temperatures and humidity ratios as well as the wall surface temperatures are collected with a data acquisition system at a sample interval of 2 s.

The average error (AE) is used to show how well the calculated results by the model compared with the experimental data during the transient response process, and is defined as:

Table 2
Initial conditions for the room model validation.

Experimental cases		
Parameters	Case I	Case II
Air-supply temperature $(t_{a,i})_o$(°C)	31.4	26.4
Air-supply humidity $(W_{a,i})_o$(g/(kg dry air))	20.3	18.1
Air temperature in the air-supply zone$(t_{a,s})_o$(°C)	32.1	28.0
Air humidity in the air-supply zone $(W_{a,s})_o$ (g/(kg dry air))	20.3	18.1
Internal surface temperature of walls in the air-supply zone $(t_{riw,s})_o$(°C)	32.7	30.2
Air temperature in the work zone $(t_{a,n})_o$(°C)	33.0	29.5
Air humidity in the work zone $(W_{a,n})_o$ (g/(kg dry air))	20.5	18.3
Internal surface temperature of walls in the work zone $(t_{riw,n})_o$(°C)	33.2	30.6
Air temperature in the air-return zone $(t_{a,r})_o$(°C)	33.1	29.9
Air humidity in the air-return zone$(W_{a,r})_o$ (g/(kg dry air))	20.5	18.3
Internal surface temperature of walls in the air-return zone $(t_{riw,r})_o$(°C)	33.6	31.1
Supply air flow rate $(G_a)_o$(kg/s)	0.15	0.20

Other parameters for the model calculation: c_a = 1005 J/(kg·°C); c_{riw} = 1250 J/(kg·°C); ρ_a = 1.18 kg/m^3; ρ_{riw} = 1800 kg/m^3; δ_{riw} = 0.22 m.

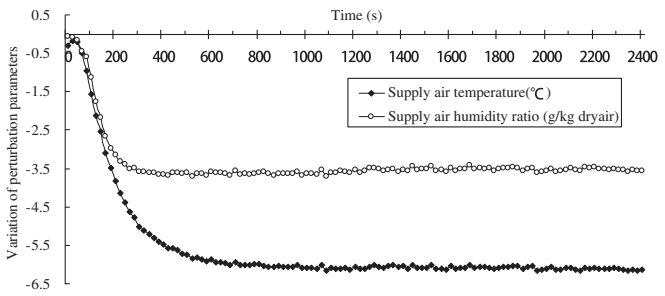

Fig. 4. Variation of perturbation parameters in the case I (measured data)

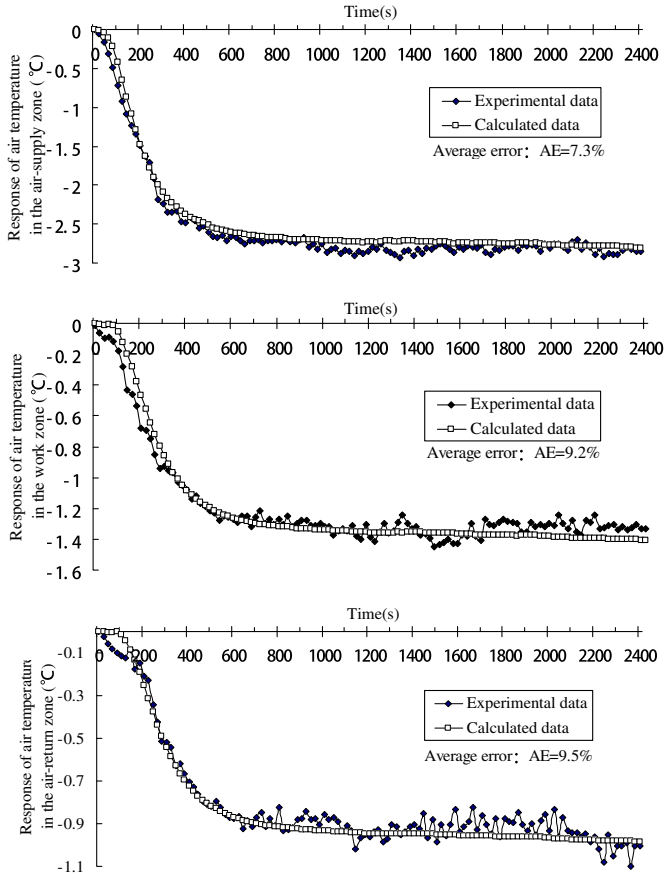

Fig. 5. Dynamic responses of air temperature in different zones in the case I (calculation vs. measurement)

$$\mathrm{AE}\left(\text{Average error}\right) = \frac{1}{N}\sum_{i=1}^{N}\left(\frac{|\Delta Y_{m,i} - \Delta Y_{\exp,i}|}{|\Delta Y_{\exp,i}|} \times 100\%\right) \qquad (35)$$

where, ΔYstands for the variation of the response parameters comparing with the initial value; the subscript 'm' and 'exp' stands for the model result and the experimental ones, respectively; *i*denotes the ith calculated or experimental result at the same time point; *N*stands for the total number of the calculated or experimental results during the transient response process.

3.3. Experimental results

3.3.1. Experimental case I

Fig. 4 shows the variation of perturbation parameters in the experimental case I, in which the supply air temperature and humidity ratio decrease to reach the steady values. The calculated

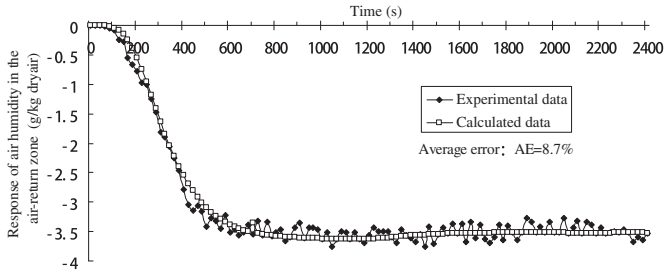

Fig. 6. Dynamic responses of air humidity in the air-return zone in the case I (calculation vs. measurement)

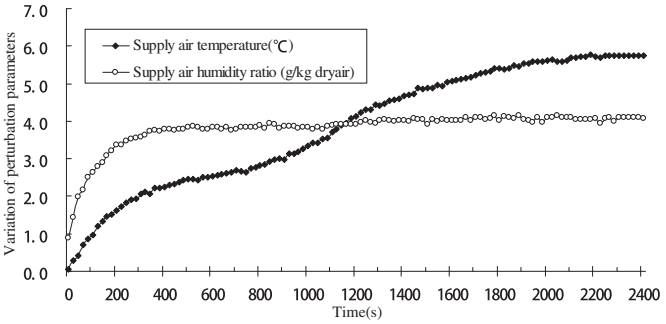

Fig. 7. Variation of perturbation parameters in the case II (measured data)

transient response of the indoor air temperatures and humidity ratios under the initial conditions of case I, and the perturbations are compared with the experimental data, which are presented in the Fig. 5 and Fig. 6. In the model calculation, the convective heat transfer coefficients are adjusted as 9.2, 11.6 and 3.2 W/(m^2 K), respectively, for the room walls, the indoor heat sources and the air layers between the adjacent indoor air zones. As easily seen from Fig. 5 and Fig. 6, the calculated response curves of the indoor air temperatures and humidity ratios are favorably consistent with the experimental ones, and the average errors of the calculated results compared with the experimental data are all lower than 10%.

3.3.2. Experimental case II

Fig. 7 shows the perturbations under the initial conditions of the case II, in which the supply air temperature and humidity ratio increase. The calculated and experimental results on the responses of the indoor air temperatures and humidity ratios are presented in Fig. 8 and Fig. 9. The average error of the calculated response of the

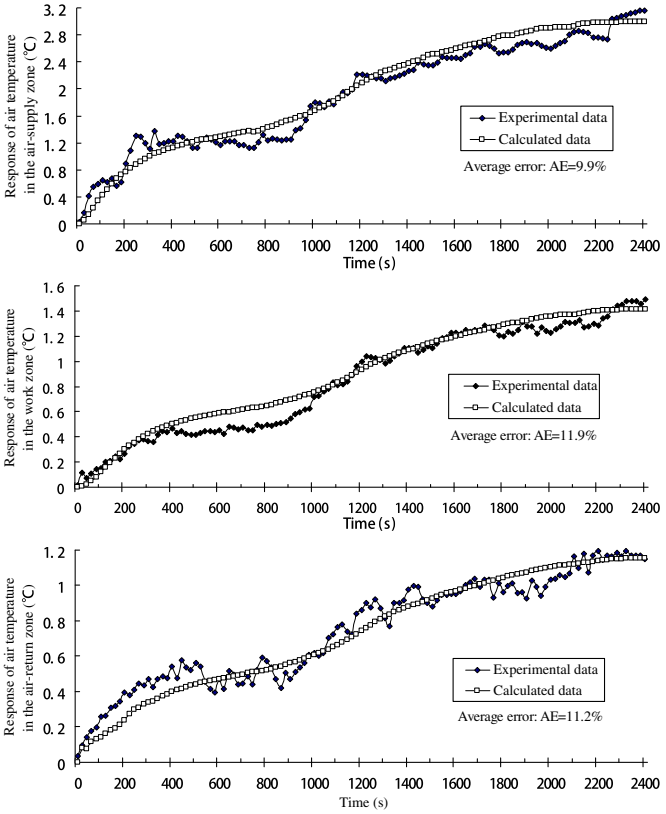

Fig. 8. Dynamic responses of air temperature in different zones in the casell (calculation vs. measurement)

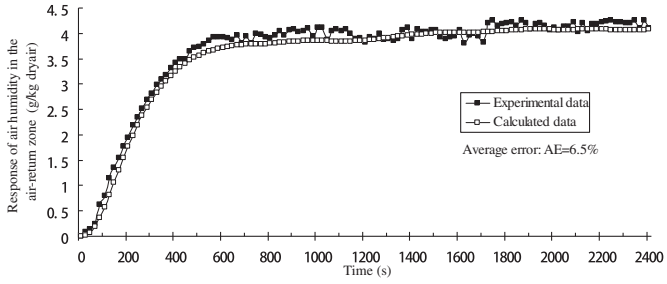

Fig. 9. Dynamic responses of air humidity in the air-return zone in the case II (calculation vs. measurement)

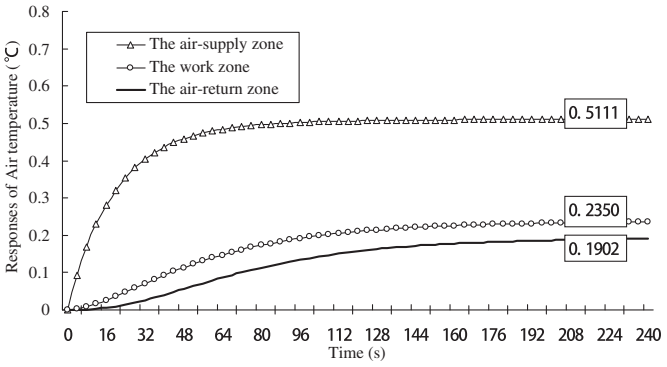

Fig. 10. Dynamic responses of air temperature in different zones when subject to a step increase of supply air temperature by 1.0 °C

air temperatures for each of the three indoor air zones is estimated as 9.9%, 11.9% and 11.2%. It was also found that the calculated response of the air humidity ratio in the air-return zone has the better agreement with the experimental data (The average error is 6.5%). In the model calculation under the case II, the heat transfer coefficients of internal wall surface and indoor heat sources as well as the air layers between the adjacent indoor air zones are adjusted respectively, as 10.7, 12.3 and 3.6 W/(m^2.K), which are a little larger than that under the case I. This is due to the higher supply air flow rate in the case II (0.20 kg/s).

The experimental cases have proven the validity of the room model developed in this study. In the following section, the transient responses of the indoor air temperatures and humidity ratios subjected to different perturbations are investigated by using the room model.

4. Simulations

The simulations are performed under the initial conditions of the case II (Table 2). The corresponding system matrixes of the model (A_{room}, B_{room}) are computed as below:

$$A_{room} = \begin{bmatrix} -0.0522 & 0 & 0.0223 & 0.0036 & 0 & 0 & 0 & 0 & 0 & 0 \\ 0 & -0.0258 & 0 & 0 & 0 & 0 & 0 & 0 & 0 & 0 \\ 0.0000 & 0 & 0.0000 & 0 & 0 & 0 & 0 & 0 & 0 & 0 \\ 0.0114 & 0 & 0 & -0.0253 & 0 & 0.0130 & 0 & 0.0007 & 0 & 0 \\ 0 & 0.0100 & 0 & 0 & -0.0100 & 0 & 0 & 0 & 0 & 0 \\ 0 & 0 & 0 & 0.0000 & 0 & -0.0000 & 0 & 0 & 0 & 0 \\ 0 & 0 & 0 & 0 & 0 & 0 & 0 & 0 & 0 & 0 \\ 0 & 0 & 0 & 0.0436 & 0 & 0 & 0 & -0.0536 & 0 & 0.0068 \\ 0 & 0 & 0 & 0 & 0.0436 & 0 & 0 & 0 & -0.0436 & 0 \\ 0 & 0 & 0 & 0 & 0 & 0 & 0 & 0.0000 & 0 & -0.0000 \end{bmatrix}$$

$$B_{room} = \begin{bmatrix} 0.0258 & 0 & -0.2062 & 0 & 0 \\ 0 & 0.0258 & 0 & 0 & 0 \\ 0 & 0 & 0 & 0 & 0 \\ 0 & 0 & -0.0752 & 0 & 0 \\ 0 & 0 & 0 & 0 & 0 \\ 0 & 0 & 0 & 0 & 0 \\ 0 & 0 & 0 & 0 & 0 \\ 0 & 0 & -0.1526 & 0 & 0 \\ 0 & 0 & 0 & 0 & 0 \\ 0 & 0 & 0 & 0 & 0 \end{bmatrix}$$

.

Two important parameters are used to describe the transient behavior of indoor air temperature and humidity ratio. One is the proportionality coefficient of response variables to the perturbation ones; the other is the time constant, i.e., the time required for the response parameters to arrive at a new steady-state after the perturbation occurs. We define the dimensionless response variable as:

$$Y^* = \frac{(Y - Y_o)}{(Y_s - Y_o)} \tag{36}$$

where, Y_o and Y_s is the initial and the steady value of the response parameter, respectively. Y is the transient value of the response parameter. In the following simulation analysis, the steady state is considered to be achieved when $Y^* = 0.95$.

4.1. Step change of supply air temperature

The transient responses of the indoor air temperatures subjected to the step increase of supply air temperature by 1.0 °C are presented in Fig. 10. According to the simulation results, the proportionality coefficient of air temperature in the three indoor zones to the step change of supply air temperature is about 0.5111 °C/°C, 0.2530 °C/°C and 0.1902 °C/°C, respectively. The corresponding time constant is estimated as 68 s, 152 s and 172 s. The results show that the perturbations of supply air temperature will produce more impact on the air temperature in the air-supply zone than on the work and air-return zones. Obviously, the perturbations of supply air temperature will not affect the indoor air humidity ratio.

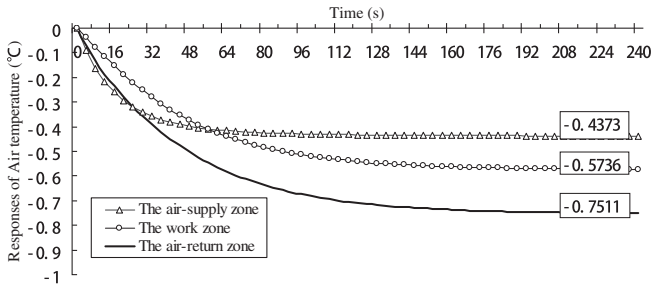

Fig. 11. Dynamic responses of air temperature in different zones when subject to a step increase of supply air flow rate by 0.1kg/s

4.2. Step change of supply air flow rate

Fig. 11 shows the transient responses of the indoor air temperatures subject to the step increase of supply air flow rate by 0.1 kg/s. Under the conditions of case II, the increase of supply air flow rate means increasing the cooling capacity of the air-conditioning system. Therefore, the indoor air temperatures will decrease when the other conditions remain unchanged. The proportionality coefficient of air temperature in the air-supply, the work and the air-return zone is estimated as −4.373 °C/(kg/s), −5.736 °C/(kg/s) and −7.511 °C/(kg/s), respectively. The corresponding time constant is about 68 s, 140 s and 140 s. This indicates that the change of supply air flow rate produces more influence on the air temperature in the work and air-return zone than on the air temperature in the air-supply zone. Fig. 12 shows the transient responses of the indoor air humidity ratio subjected to a step increase of 0.1 kg/s in the supply air flow rate. It is shown that the air humidity ratio in the work zone and in the air-supply zone shares a similar response characteristic as the air temperature. The proportionality coefficient and time constant of response is about −0.992 (g/kg dry air)/(kg/s) and 320 s, respectively. However, the air humidity ratio in the air-supply zone has no response to the perturbations of supply air flow rate. This is because there is no moisture load in the air-supply zone. Meanwhile, the air humidity ratio in the air-supply zone is not affected by the air in the other zones.

4.3. Step change of indoor occupant number

The dynamic responses of air temperature and humidity ratio subjected to a step increase of occupant number are also investigated. In the model, the change of indoor occupant number is realized by adjusting indoor occupants' area. Fig. 13 and Fig. 14 present the calculated responses of indoor air conditions (i.e., temperatures and humidity ratios) when the total area of occupant indoors increases by 10 m^2. As the results show, the air conditions in the work zone is mostly affected by the perturbations of indoor occupants, and then followed by that in the air-return and air-supply zone. The results also indicate that the change of indoor occupant number produces much greater influence on the indoor air temperatures than it does on the indoor air humidity ratios.

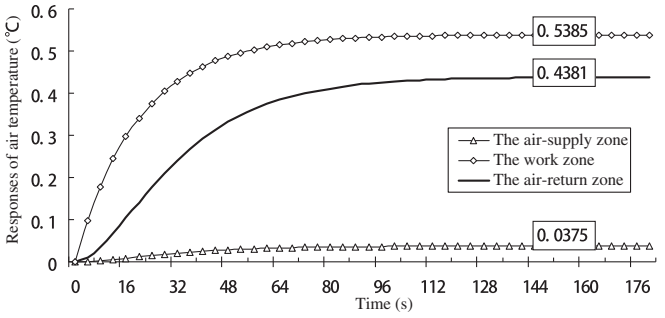

Fig. 13. Dynamic responses of air temperature in different zones when subject to a step increase of occupant number ($A^{(1)}_{rq,n}\uparrow 10\ m^2$)

4.4. Step change of ambient temperature

The ambient temperature affects indoor thermal environment mainly through the external building envelopes. For the convenience of the simulation, we assume the external envelopes of the room with the surface area of 10 m^2 and the thickness of 0.3 m. The convective heat transfer coefficient and the solar radiation absorption coefficient of the walls' external surface is considered as 13.5 W/(m^2.°C) and 0.65, respectively. The initial ambient temperature is 33.0 °C and the initial solar radiation intensity on the external walls is 400 W/m^2. The other initial conditions can be referred to the case II (Table 2). The influences of the thermal insulation of the external walls and the perturbations of the ambient temperature on the indoor thermal responses are studied as shown in Fig. 15 for a step increase of ambient temperature by 1.0 °C. It was found that the response time of the indoor air temperatures subjected to the ambient perturbations is much longer than that to all the other perturbations including the supply air conditions, the supply air flow rate and the indoor heat load. Meanwhile, a better thermal insulation of the external wall contributes to a smaller influence of the ambient perturbations on the indoor air temperatures. In comparison, the indoor air humidity ratio does not response to the change of ambient temperature in this case.

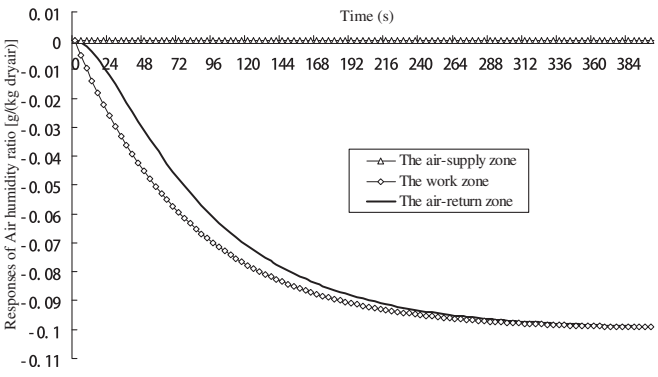

Fig. 12. Dynamic responses of air humidity ratio in different zones when subject to a step increase of supply air flow rate by 0.1kg/s

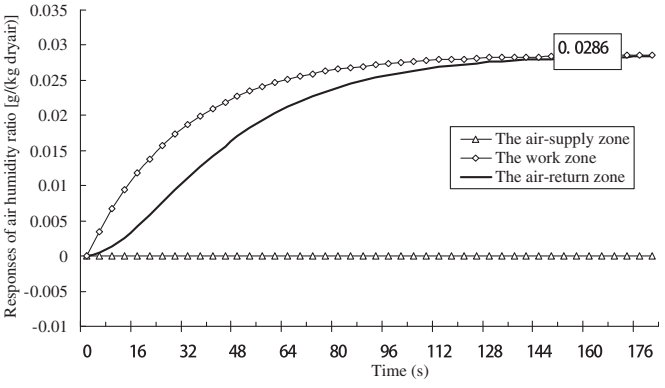

Fig. 14. Dynamic responses of air humidity ratio in different zones when subject to a step increase of occupant number ($A^{(1)}_{rq,n}\uparrow 10\ m^2$)

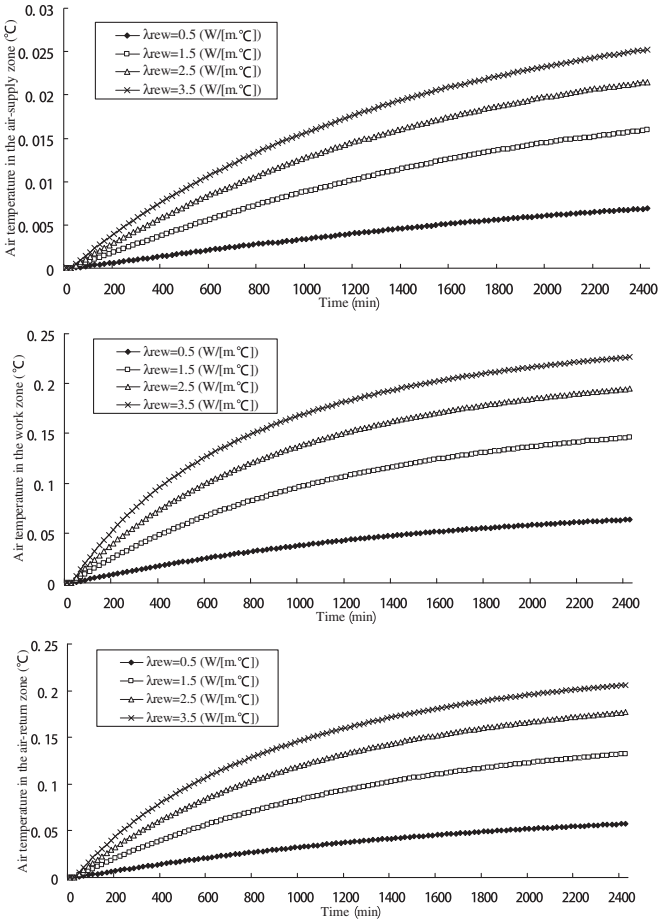

Fig. 15. Dynamic responses of air temperature in different zones when subject to a step increase of ambient temperature by 1.0 °C

5. Conclusions

This paper presents a three-zone dynamic state-space room model for the study of the dynamic thermal response of air in rooms. Through reasonable linearization, the model is transformed into the state-space representation. Experiments have been performed to validate the room model in terms of the 2400-s dynamic responses of indoor air thermal conditions subject to the perturbations of supply air temperature and humidity ratio. The average errors of the calculated response results compared with the experimental data are all lower than 12%, which indicates that the state-space model developed in this study provides satisfactory and realistic predictions on the dynamic responses of indoor thermal conditions to different perturbations.

The state-space model can be conveniently described by a directed graph, and the analytical solution to the state equation can be obtained easily. Therefore, the room model developed in this study is a fast and accurate method to provide detailed quantitative and qualitative analyses on the relationship between the indoor air conditions and the ambient perturbations.

Frankly, the model developed in this study is not perfect enough. Some potential factors, e.g., the influences of solar radiation through window and the irradiative temperature, haven't been considered in the model. But, it doesn't affect the proposed modeling approach itself. Further extension possibilities of the room state-space model regarding these aspects can be conveniently realized without changing the model representation. The room air zone division is the key step for the model applications, which may affect the model results to some extent. In the future work, the HVAC controller based on the state-space model will be studied.

Acknowledgements

This work was supported by a grant from the National Natural Science Foundation of China (No. 51076100) and Project of International Cooperation and Exchanges NSFC (No. 51110105012).

References

[1] Metha DP, Woods JE. An experimental validation of a rational model of dynamic responses of building. ASHRAE Transactions 1980;86(1):546–58.
[2] Borresen BA. Thermal room models for control analysis. ASHRAE Transactions 1981;87(2):251–60.
[3] Roberts AS, Oak MP. Nonlinear dynamics and control for thermal room models. ASHRAE Transactions 1991;97(1):722–8.
[4] Ahmed O, Mitchell JW, Klein SA. Experimental validation of thermal and pressure models in a laboratory simulator. ASHRAE Transactions 1998;104(2):983–96.
[5] Yang IH, Kim KW. Prediction of the time of room air temperature descending for heating systems in buildings. Building and Environment 2004;39(1):19–29.
[6] Mustafaraj G, Chen J, Lowry G. Development of room temperature and relative humidity linear parametric models for an open office using BMS data. Energy and Buildings 2010;42(3):348–56.
[7] Wu S, Sun JQ. A physics-based linear parametric model of room temperature in office buildings. Building and Environment 2012;50(4):1–9.
[8] Orosa JA, Oliveira AC. Software tools for HVAC research. Advances in Engineering Software 2011;42(10):846–51.
[9] Murakami S, Kato S, Kim T. Indoor climate design based on CFD coupled simulation of convection, radiation, and HVAC control for attaining a given PMV value. Building and Environment 2001;36(6):701–9.
[10] Chen Q, Srebric J. A procedure for verification, validation, and reporting of indoor environment CFD analyses,. HVAC&R Research 2002;8(2):201–16.
[11] Cheong KWD, Djunaedy E, Chua YL, Tham KW, Sekhar SC, Wong NH, et al. Thermal comfort study of an air-conditioned lecture theatre in the tropics. Building and Environment 2003;38(1):63–73.
[12] Wang L, Chen Q. Theoretical and numerical studies of coupling multizone and CFD models for building air distribution simulations. Indoor Air 2007;17(5):348–61.
[13] Catalina T, Virgone J, Kuznik F. Evaluation of thermal comfort using combined CFD and experimentation study in a test room equipped with a cooling ceiling. Building and Environment 2009;44(8):1740–50.
[14] Maxime TG, Louis G. Comfort and energy consumption of hydronic heating radiant ceilings and walls based on CFD analysis. Building and Environment 2012;54(8):1–13.
[15] Chen Q, Peng X, van Paassen AHC. Prediction of room thermal response by CFD technique with conjugate heat transfer and radiation models. ASHRAE Transactions 1995;101(part 1):50–60.
[16] Zerihun Desta T, Janssens K, Van Brecht A, Meyers J, Baelmans M, Berckmans D. CFD for model-based controller development. Building and Environment 2004;39(6):621–33.
[17] Sun Z, Wang S. A CFD-based test method for control of indoor environment and space ventilation. Building and Environment 2010;45(6):1441–7.
[18] Inard C, Bouia H, Dalicieux P. Prediction of air temperature distribution in buildings with a zonal model. Energy and Buildings 1996;24(2):125–32.
[19] Peng X, van Paassen AHC. A state space model for predicting and controlling the temperature responses of indoor air zones. Energy and Buildings 1998;28(1):197–203.
[20] Kasahara M. Yoshiaki Kuzuu, Tadahiko Matsuba. Physical model of an air-conditioned space for control analysis. ASHRAE Transactions 2000;106(2):304–17.
[21] Riederer P, Marchio D, Visier JC, Husaunndee A. Room thermal modeling adapted to the test of HVAC control systems. Building and Environment 2002;37(9):777–90.
[22] Moroşan Petru-Daniel, Bourdais Romain, Dumur Didier, Buisson Jean. Building temperature regulation using a distributed model predictive control. Energy and Buildings 2010;42(9):1445–52.
[23] Prívara Samuel, Široký Jan, Širok Jan, Cigler Jiří. Model predictive control of a building heating system: the first experience. Energy and Buildings 2011;43(2–3):564–72.
[24] Hazyuk Ion, Ghiaus Christian, Penhouet David. Optimal temperature control of intermittently heated buildings using model predictive control: Part II – control algorithm. Building and Environment 2012;51(5):388–94.

[25] ASHRAE. ASHRAE handbook–fundamentals, chapter 8. Atlanta: American Society of Heating, Refrigerating and Air-Conditioning Engineers, Inc.; 2005.
[26] Ministry of Construction of PR China. Code for design of heating ventilation and air conditioning (GB50019-2003). Beijing: Plans Press of China; 2003.
[27] Liu W, Lian Z, Yao Ye. Optimization on indoor air diffusion of floor-standing type room air-conditioners. Energy and Buildings 2008;40(2): 59–70.
[28] Gao J, Zhang X, Zhao JN, Gao FS. A heat transfer parameter at air interfaces in the BLOCK model for building thermal environment. International Journal of Thermal Sciences 2010;49(2):463–70.
[29] Diestel Reinhard. Graph theory. 4th ed. Heidelberg (Germany): Springer-Verlag; 2010.
[30] Friedland Bernard. Control system design: an introduction to state space methods. Dover Publications (USA); 2005.